doi:10.1038/nature10137

Supplementary Table 1 | YAP signature used in Supplementary Fig. 2
Contains the genes commonly upregulated by YAP in human MCF10A cells, mouse NIH3T3 cells and mouse liver as obtained from the merging of data published in Refs.[36-38].

Probeset	Gene
203002_at	AMOTL2
206029_at	ANKRD1
1552619_a_at	ANLN
222608_s_at	ANLN
1560318_at	ARHGAP29
202686_s_at	AXL
213429_at	NA
202095_s_at	BIRC5
1554283_at	CCRN4L
202870_s_at	CDC20
224847_at	CDK6
204159_at	CDKN2C
209172_s_at	CENPF
222073_at	COL4A3
216898_s_at	COL4A3
202551_s_at	CRIM1
209101_at	CTGF
210764_s_at	CYR61
201289_at	CYR61
201278_at	DAB2
201280_s_at	DAB2
210757_x_at	DAB2
201279_s_at	DAB2
209094_at	DDAH1
224790_at	ASAP1
221039_s_at	ASAP1
224791_at	ASAP1
210762_s_at	DLC1
224822_at	DLC1
201044_x_at	DUSP1
208955_at	DUT
219787_s_at	ECT2
225078_at	EMP2
204975_at	EMP2
225079_at	EMP2
203348_s_at	ETV5
204422_s_at	FGF2
204421_s_at	FGF2
213746_s_at	FLNA
201564_s_at	FSCN1
208782_at	FSTL1
209305_s_at	GADD45B
238756_at	GAS2L3
202177_at	GAS6
203560_at	GGH
234192_s_at	GKAP1
223378_at	GLIS2
211414_at	GLS
223079_s_at	GLS
221510_s_at	GLS
201944_at	HEXB
207165_at	HMMR
222126_at	AGFG2
1555349_a_at	ITGB2
202803_s_at	ITGB2
201125_s_at	ITGB5
218656_s_at	LHFP
232168_x_at	MACF1
201668_x_at	MARCKS
217599_s_at	MDFIC
1554126_at	MSRB3
225790_at	MSRB3
225080_at	MYO1C
200632_s_at	NDRG1
219165_at	PDLIM2
201397_at	PHGDH
210139_s_at	PMP22
204030_s_at	SCHIP1
222717_at	SDPR
218711_s_at	SDPR
202627_s_at	SERPINE1
229674_at	SERTAD4
235579_at	SFRS2IP
201739_at	SGK1
219749_at	SH2D4A
219493_at	SHCBP1
230130_at	SLIT2
209897_s_at	SLIT2
200783_s_at	STMN1
220407_s_at	TGFB2
209908_s_at	TGFB2
228121_at	TGFB2
209909_s_at	TGFB2
211573_x_at	TGM2
201042_at	TGM2
201109_s_at	THBS1
201108_s_at	THBS1
201110_s_at	THBS1
202338_at	TK1
215389_s_at	TNNT2
218864_at	TNS1
201292_at	TOP2A
200973_s_at	TSPAN3

Supplementary Table 2 | sequences of siRNA used in this study

siRNA	SENSE STRAND SEQUENCE
YAP 1	GACAUCUUCUGGUCAGAGA dTdT
YAP 2	CUGGUCAGAGAUACUUCUU dTdT
TAZ 1	ACGUUGACUUAGGAACUUU dTdT
TAZ 2	AGGUACUUCCUCAAUCACA dTdT
LATS1 A	CACGGCAAGAUAGCAUGGA dTdT
LATS1 B	CAUACGAGUCAAUCAGUAA dTdT
LATS2 A	AAAGGCGUAUGGCGAGUAG dTdT
LATS2 B	GCCACGACUUAUUCUGGAA dTdT
Control	UUCUCCGAACGUGUCACGU dTdT

YAP/TAZ mix #1 is composed of oligos YAP1 and TAZ1; YAP/TAZ mix #2 is composed of oligos YAP2 and TAZ2; LATS1/2 mix A is composed of oligos LATS1A and LATS2A; LATS1/2 mix B is composed of oligos LATS1B and LATS2B.

Supplementary Table 3 | sequences of RT-PCR primers used in this study

GENE	PRIMER NAME	PRIMER SEQUENCE
GAPDH	GAPDH F	CTCCTGCACCACCAACTGCT
	GAPDH R	GGGCCATCCACAGTCTTCTG
ANKRD1	ANKRD1 FOR	AGTAGAGGAACTGGTCACTGG
	ANKRD1 REV	TGGGCTAGAAGTGTCTTCAGAT
CTGF	CTGF F2	AGGAGTGGGTGTGTGACGA
	CTGF R2	CCAGGCAGTTGGCTCTAATC
LATS1	LATS1 L1	CTCTGCACTGGCTTCAGATG
	LATS1 R1	TCCGCTCTAATGGCTTCAGT
LATS2	LATS2 L1	ACATTCACTGGTGGGGACTC
	LATS2 R1	GTGGGAGTAGGTGCCAAAAA

Primers used for the molecular characterization of hMSC differentiation were as in Ref.[12].

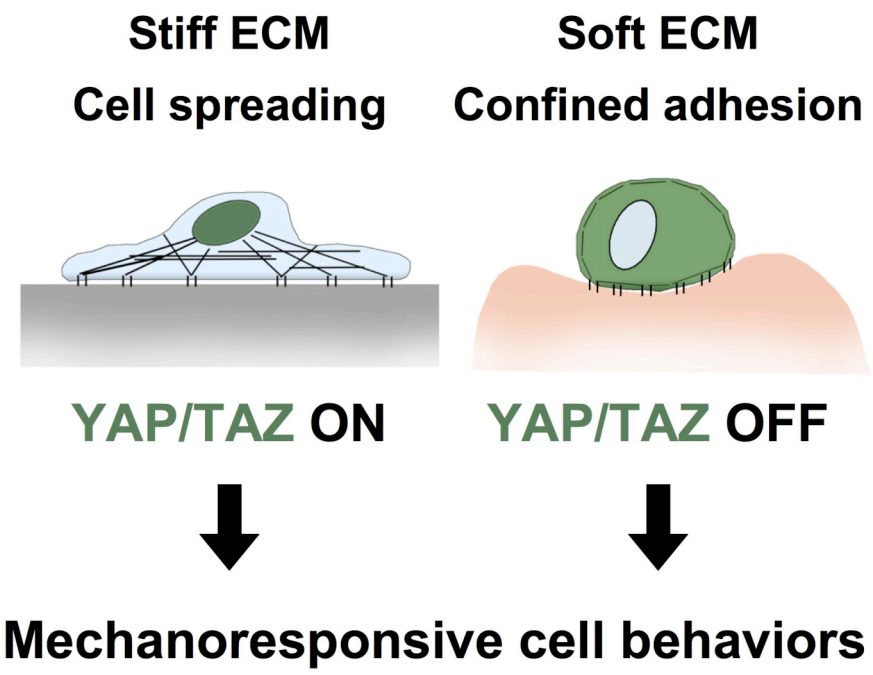

Supplementary Figure 1 | A model for the role of YAP/TAZ as readers and effectors of cell behavior induced by the mechanical/physical properties of the cellular microenvironment, such as ECM stiffness, cell spreading and cytoskeletal tension. On the left: Cells growing on stiff substrates (indicated in grey) can develop cytoskeletal tension by pulling on the ECM, which permits the maturation of cell-substrate adhesions[3] (indicated by the symbol ||) and the development of stress-fibers (indicated by the black lines in the cytoplasm). In these conditions, YAP/TAZ transcriptional coactivators (indicated in green) accumulate in the nucleus and can regulate gene transcription, enabling cells to behave according to the mechanical microenvironment. On the right: Cells growing on soft substrates (indicated in pink) cannot develop cytoskeletal tension and display reduced or no stress-fibers (black lines abutting the cell membrane indicate the formation of the cortical F-actin cytoskeleton). In these conditions, YAP/TAZ are excluded from the nucleus and accumulate in the cytoplasm (now stained in green). In this case, it is the absence of YAP/TAZ transcriptional activity that instructs cell behavior in response to the microenvironment.

signaling pathway	p-value
TGF-beta[a]	0.997
TGF-beta[b]	0.286
Ras	0.170
ERBB2	0.551
YAP/TAZ	**$< 10^{-5}$**
YAP	**$< 10^{-5}$**
Wnt	not represented
beta-catenin	not represented
Notch	0.997
NICD	0.997
NF-kappaB	0.997
MAL/SRF[a]	0.086
MAL/SRF[b]	0.125

Supplementary Figure 2 | Over-representation of YAP/TAZ target genes among the genes regulated by substrate stiffness in NMuMG mouse Mammary Epithelial Cells (MEC). Over-representation analysis was performed using one-sided Fisher's exact test (p-value<0.05). p-values were adjusted for False Discovery Rate (FDR<5%) (see Methods). Gene-sets highlighting activation of specific signaling pathways were derived from previously defined gene-expression signatures (see Methods for Refs.). Genes of WNT and β-catenin signatures were not represented in the stiffness signature. In yellow: over-representation reaches statistical significance only for the YAP/TAZ signatures.

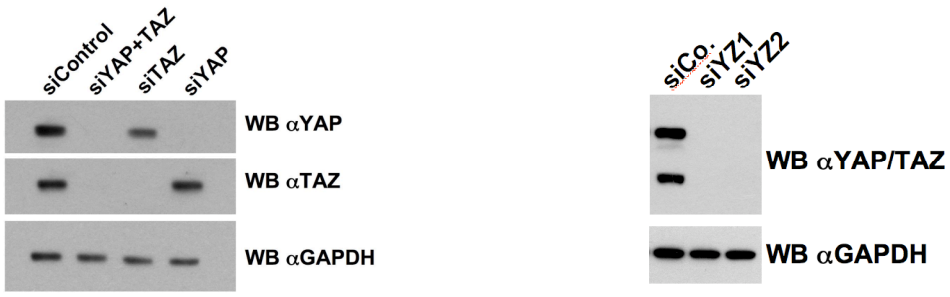

Supplementary Figure 3a | LEFT PANEL: Lysates of MCF10A cells transfected with the indicated siRNAs (siYAP #1 and siTAZ #1) and subjected to western blotting to ensure specific depletion of the endogenous proteins. RIGHT PANEL: Western blotting of MCF10A with an anti-YAP/TAZ antibody shows comparable quantitative knockdown of YAP (upper band) and TAZ (lower band) endogenous protein levels by two independent YAP/TAZ siRNA sets (siYZ1 and siYZ2), as compared to cells transfected with control siRNA (siCo.).

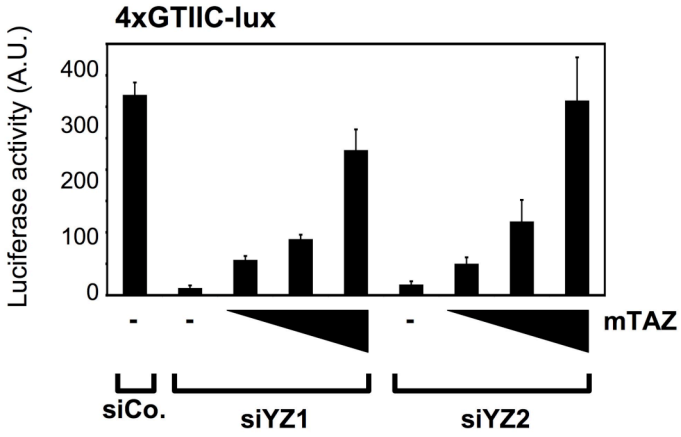

Supplementary Figure 3b | MDA-MB-231 cells were transfected with control siRNA (siCo.) or with two combinations of YAP/TAZ siRNA (siYZ1 and siYZ2); the day after, cells were transfected with 4xGTIIC-lux reporter and with increasing doses of mTAZ expression plasmid (insensitive to siRNAs against hTAZ) as indicated. Both YAP/TAZ siRNAs combinations down-regulate YAP/TAZ activity, and this is rescued by mouse TAZ, showing specificity of the YAP/TAZ depletion. Data are mean and SD (n=6).

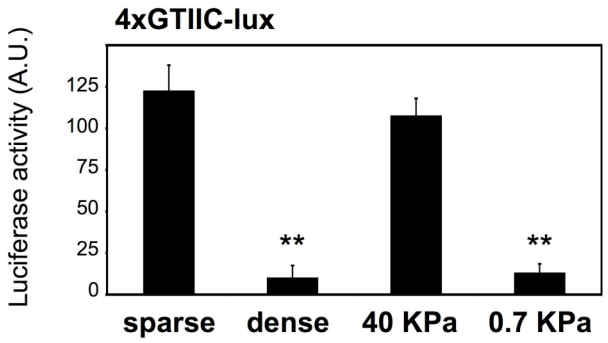

Supplementary Figure 4 | The activity of a YAP/TAZ-responsive synthetic promoter driving luciferase expression is similarly regulated by high confluence and by substrate rigidity in HeLa cells. Cells were transfected with 4xGTIIC-lux reporter and plated at low or high confluence (sparse and dense respectively) on plastics, and at low confluence on stiff (40 KPa) or soft (0.7 KPa) fibronectin-coated hydrogels. Data are presented as mean and SD (n=6; $**P<0.01$).

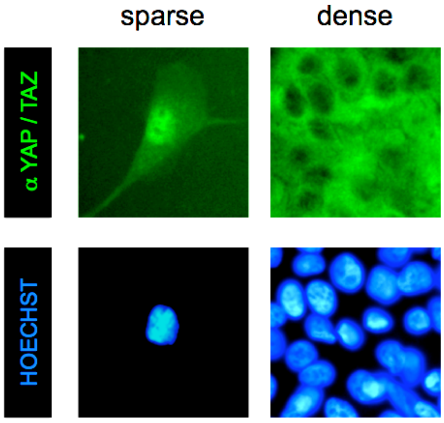

Supplementary Figure 5 | Confocal IF images for endogenous YAP/TAZ and nuclei (Hoechst) of human MEC plated at low (sparse) or high (dense) confluence for 48 hours.

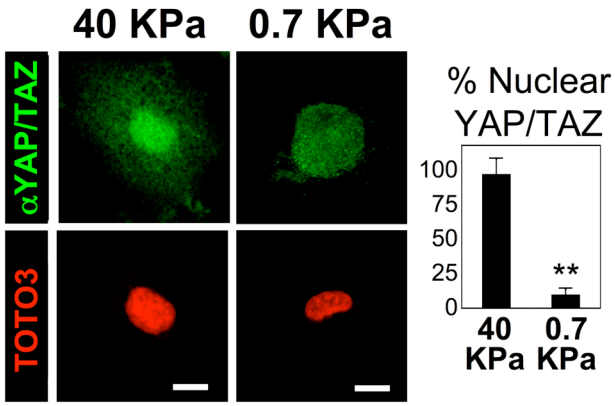

Supplementary Figure 6 | ECM stiffness regulates YAP/TAZ nuclear localization. Confocal immunofluorescence (IF) images of YAP/TAZ (green) and nuclei (red) of NMuMG MEC plated on stiff (40KPa) and soft (0.7KPa) fibronectin-coated acrylamide hydrogels. White bars = 15μm. Graphs on the right indicate the ratio of cells with nuclear YAP/TAZ; data are mean and SD (n=3; ***P*<0.01).

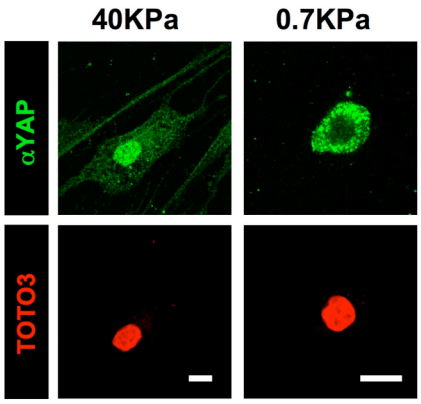

Supplementary Figure 7 | Relocalization of endogenous YAP in hMSC plated on stiff (40 KPa) and soft (0.7 KPa) matrices as seen by confocal IF by using an alternative anti-YAP antibody to that used in other panels. TOTO3 staining identifies nuclei. White bars = 15 μm.

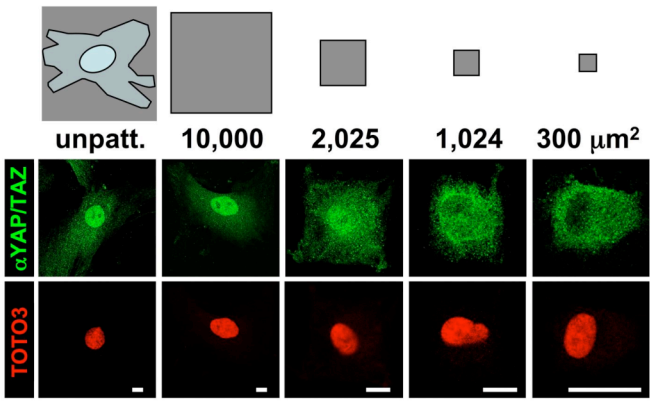

Supplementary Figure 8 | This refers to Figure 1c of the main text. Confocal IF images of endogenous YAP/TAZ (also shown in Fig. 1c) together with their corresponding nuclei (TOTO3) in hMSC plated on microprinted fibronectin islands of decreasing size. White bars = 15μm.

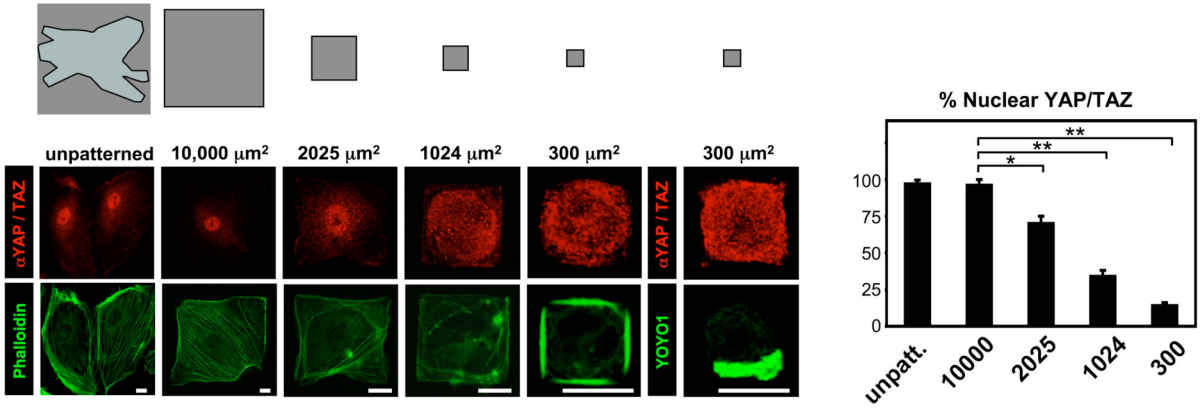

Supplementary Figure 9 | This refers to Figure 1d of the main text. Constraining cell shape regulates YAP/TAZ nuclear localization also in Human Microvascular Endothelial Cells (HMVEC). Confocal IF images of endogenous YAP/TAZ and actin filaments (phalloidin) in HMVEC plated on microprinted fibronectin islands of decreasing size (μm^2). White bars = 15μm. On the right: IF images of YAP/TAZ and the nucleus (YOYO1) of a cell plated on the smallest island. The pictures of cells plated on 10,000 and 300 μm^2 are the same of Fig. 1d, shown here with representative cells on islands of intermediate sizes for completeness. Right graphs provide complete quantifications. Data are mean and SD (n=7; **P*<0.05, ***P*<0.01).

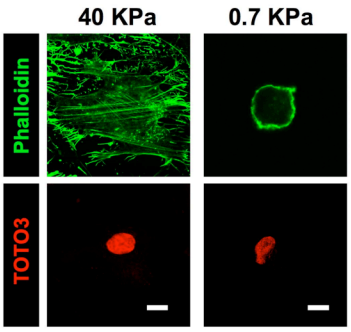

Supplementary Figure 10 | Confocal IF images of hMSC plated on substrate of different stiffness (40 and 0.7 KPa) and stained for F-actin (Phalloidin) and nuclei (TOTO3). White bars = 15 μm.

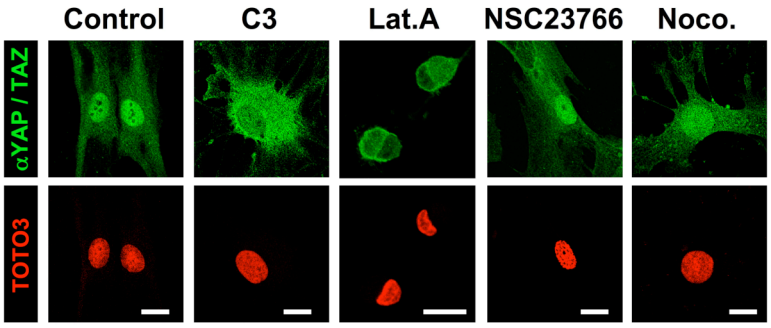

Supplementary Figure 11 | IF images of hMSC shown in Fig. 2a, here presented with their corresponding nuclear stainings (TOTO3).

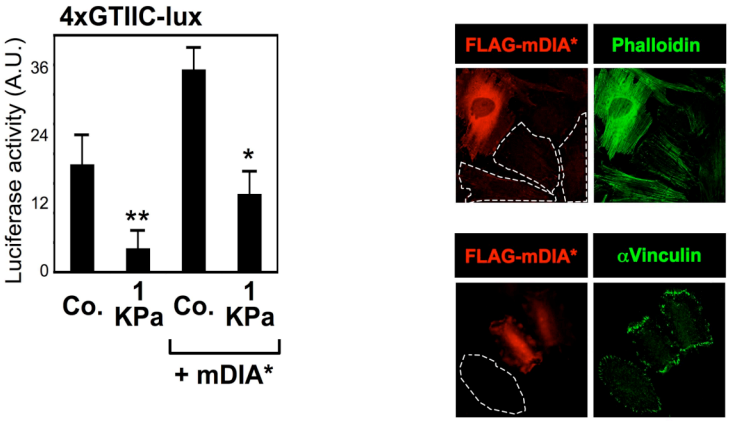

Supplementary Figure 12 | LEFT: Overexpression of activated Diaphanous (mDIA*) enhances YAP/TAZ transcriptional activity as assayed by luciferase activity in HeLa cells plated on plastics (Co.) or on soft ECM (1 KPa). Data are mean and SD (n=3; **P*<0.05, ***P*<0.01). RIGHT, Upper panel: confocal IF images of HeLa cells transiently transfected with activated Diaphanous (FLAG-mDIA*). Transfected cells are stained with anti-FLAG (red channel). Staining with Phalloidin (green channel) shows enhanced stress-fibers in cells expressing active Diaphanous. Cells encircled by white dotted lines are non-transfected cells displaying background anti-FLAG staining and serve as internal controls. RIGHT, Lower panel: confocal IF images of HeLa cells transiently transfected with activated Diaphanous and mCherry as tracer (red channel) and stained for focal adhesions (Vinculin – green channel). Enhanced vinculin recruitment to focal adhesions in cells expressing mDIA* is suggestive of increased cytoskeletal tension[30,31].

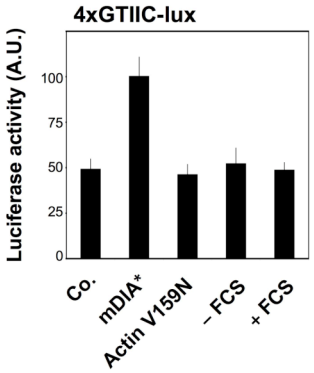

Supplementary Figure 13 | Overexpression of actin V159N and serum stimulation are unable to enhance YAP/TAZ. HeLa cells were transfected with 4xGTIIC-lux reporter together with empty vector (Co.), with activated Diaphanous (mDIA*), with a plasmid encoding for V159N actin, or starved overnight without serum (- FCS) and subsequently treated with 20% serum (+ FCS). Data are mean and SD (n=5).

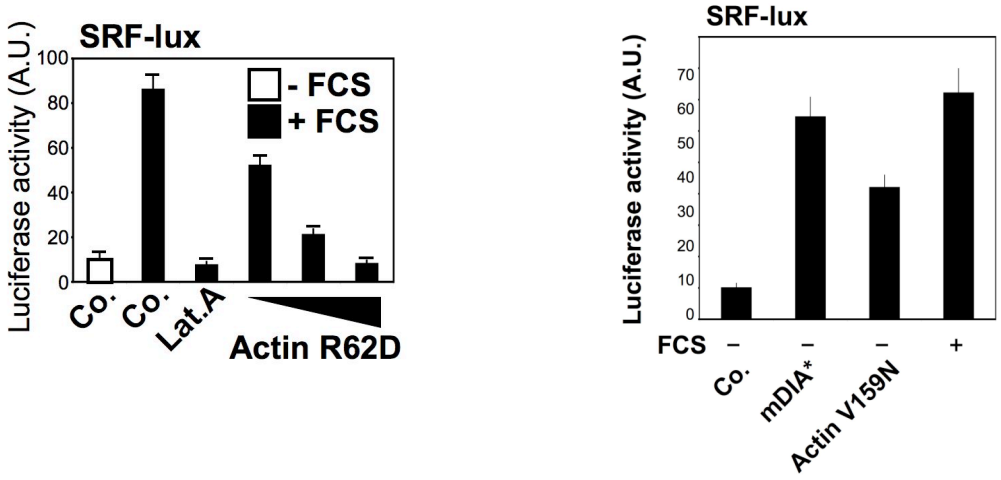

Supplementary Figure 14 | Positive controls for the activity of the R62D and V159N actin mutants used in Fig. 2c and Supplementary Fig. 13. LEFT: MAL/SRF-responsive element (SRF-lux) activity in HeLA cells treated as indicated and trasfected with R62D actin, using the same plasmid doses as in Fig. 2c. RIGHT: HeLa cells transfected with SRF-lux, showing effective enhancement of MAL/SRF activity upon expression of mDIA*, V159N actin and FCS (20% serum) stimulation. Plasmid doses used were the same as in Supplementary Fig. 13. Co. indicates transfection with empty vector. All data are mean and SD (n=5).

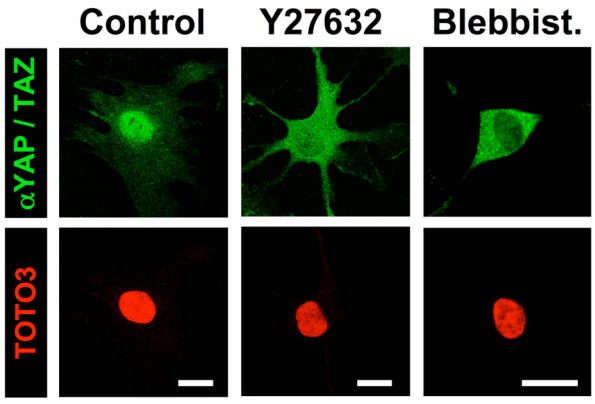

Supplementary Figure 15 | IF images of hMSC shown in Fig. 2d, here presented with their corresponding nuclear stainings (TOTO3).

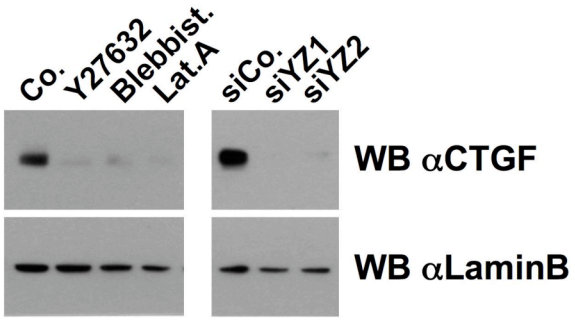

Supplementary Figure 16 | Western blots for endogenous CTGF protein levels in MDA-MB-231 cells untreated (Co.), treated with the indicated inhibitors of ROCK (Y27632), Myosin (Blebbistatin) and F-actin (LatrunculinA), or transfetced with the indicated siRNAs. LaminB ensures uniform loading.

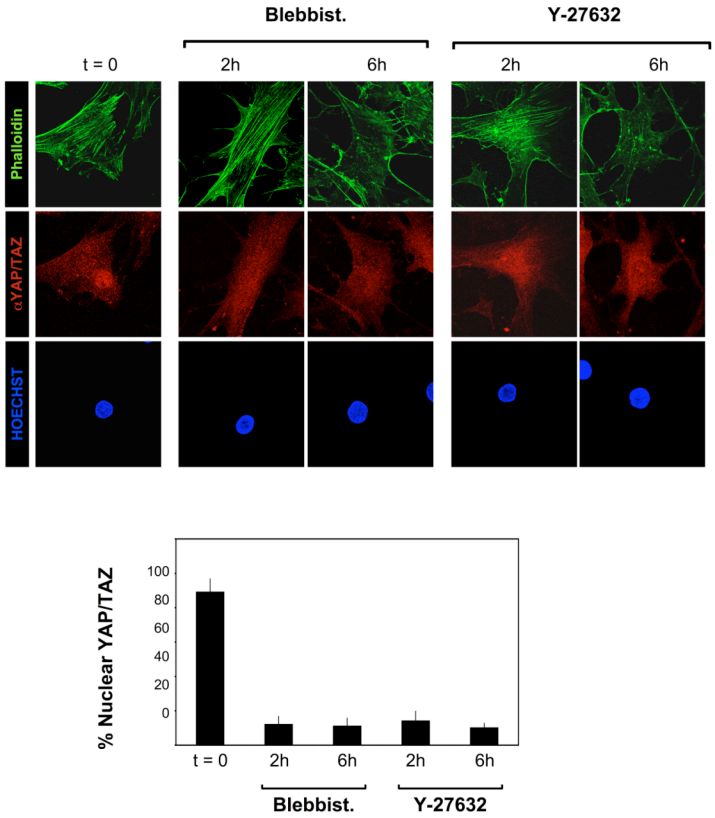

Supplementary Figure 17 | Confocal IF images of hMSC cells plated on fibronectin-coated glass slides and treated for different periods (2 and 6 hours, respectively) with the indicated inhibitors of ROCK (Y27632) or non-muscle myosin (Blebbistatin). Cells were stained for YAP/TAZ (red channel), F-actin (Phalloidin – green channel) and nuclei (Hoechst – blue channel). Graphs provide the quantifications of nuclear YAP/TAZ. Data are mean and SD (n=3). Note how inhibition of cytoskeletal tension after 2 hours influences YAP/TAZ localization before affecting stress-fiber integrity.

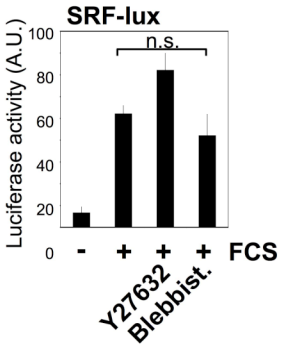

Supplementary Figure 18 | Cytoskeletal tension marginally sustains MAL/SRF activity. HeLa cells were transfected with a MAL/SRF-responsive element reporter (SRF-lux), left for 24h in the absence of serum (fetal calf serum, FCS), and subsequently supplemented (+) of serum (20%) without or with the indicated inhibitors of ROCK (Y27632 50μM) and non-muscle myosin II (Blebbistatin 50μM) for 6 more hours. Data are mean and SD; n.s. not statistically significant (n=2).

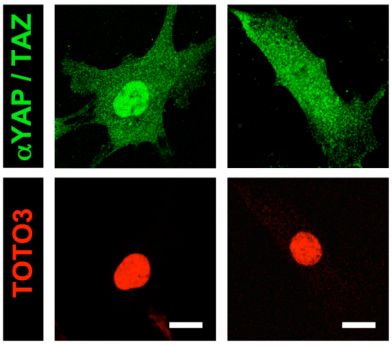

Supplementary Figure 19 | IF images of hMSC shown in Fig. 2f, here presented with their corresponding nuclear stainings (TOTO3).

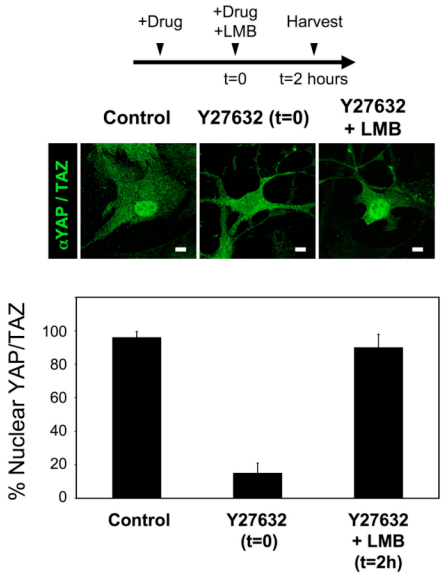

Supplementary Figure 20a | YAP/TAZ localization is regulated by cytoskeletal tension at the level of nuclear retention. YAP/TAZ confocal immunofluorescent microscopy of hMSC plated on fibronectin-coated slides and treated with the ROCK inhibitor Y27632 to exclude YAP/TAZ from nuclei (t=0) and then also treated with the inhibitor of CRM1-dependent nuclear export Leptomycin B (LMB, 40ng/ml) for 2 additional hours. Quantifications are shown as mean and SD (n=3). LMB treatment restores YAP/TAZ nuclear localization in cells with relaxed acto-myosin cytoskeleton. Similar results were obtained by treating cells with the Rho inhibitor C3 (not shown). White bars = 15μm.

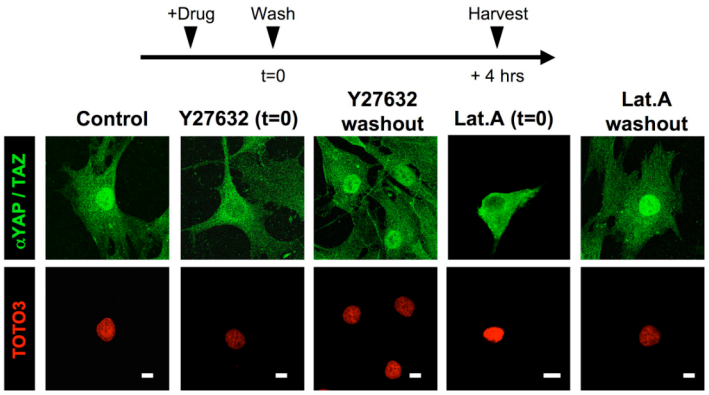

Supplementary Figure 20b | Confocal IF pictures of hMSC that were plated on fibronectin-coated glass, and treated with the indicated small molecule inhibitors to cause YAP/TAZ exclusion (t=0). Y27632 is a ROCK inhibitor; LatrunculinA (Lat.A) is an F-actin inhibitor. Inhibitors were then removed (washout) and cells were incubated in normal medium for 4 more hours before fixation. White bars = 15 μm.

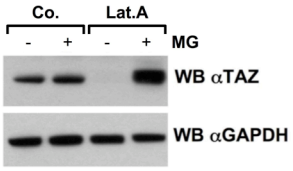

Supplementary Figure 21 | LatrunculinA treatment induces proteasomal-dependent degradation of TAZ. Human MEC were either untreated (Co.) or treated 4 hours with LatrunculinA (Lat.A) , without (-) or with (+) the addition of the proteasome inhibitors MG132/MG115 (MG - 10μM each) and then harvested for western blotting.

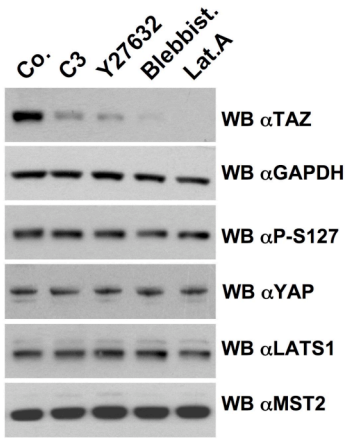

Supplementary Figure 22 | Treatment of hMSC with Rho inhibitor C3 or with cytoskeletal inhibitors as in Fig. 2a or 2d causes TAZ degradation, as assayed by western blotting of cell lysates. Note how the levels of YAP serine127 phosphorylation (P-S127, a readout of LATS kinase activity) were not increased. Also the stability of YAP, LATS1 and MST2 was not affected.

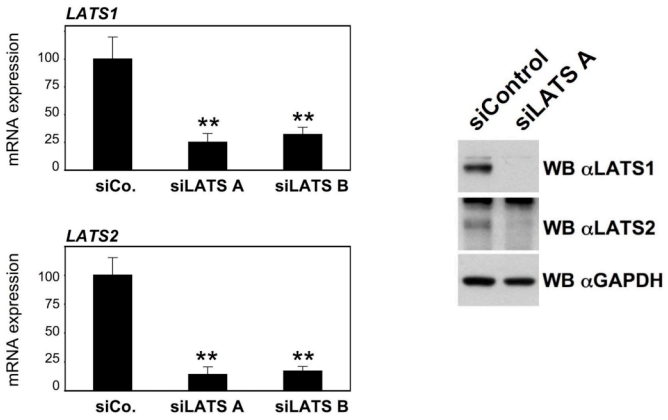

Supplementary Figure 23a | Human MEC were transfected with two independent sets of siRNA targeting LATS1 and LATS2, and analyzed by qRT-PCR (left panels) or western blotting (WB – right panels) to prove efficient knockdowns of the endogenous mRNA and proteins (similar WB results were obtained with siLATS B). Data are mean and SD (n=3; $**P<0.01$).

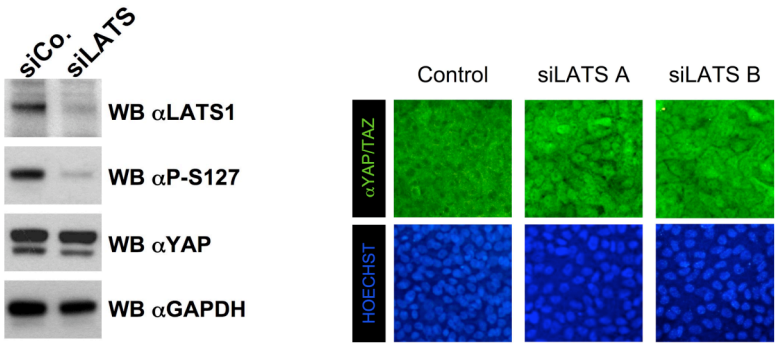

Supplementary Figure 23b | LEFT: Human MEC were transfected with the indicated siRNA, replated at low confluence and cultivated for 2 days before harvesting for western blotting. Upon LATS knockdown, YAP phoshorylation on serine127 is also decreased. Similar results were obtained with siLATS B. RIGHT: Human MEC were transfected with the indicated siRNA and replated at high confluence. After 2 days cells were analyzed for endogenous YAP/TAZ localization by immunofluorescence microscopy. Cell nuclei were visualized by Hoechst staining. Note the increased nuclear staining upon LATS knockdown.

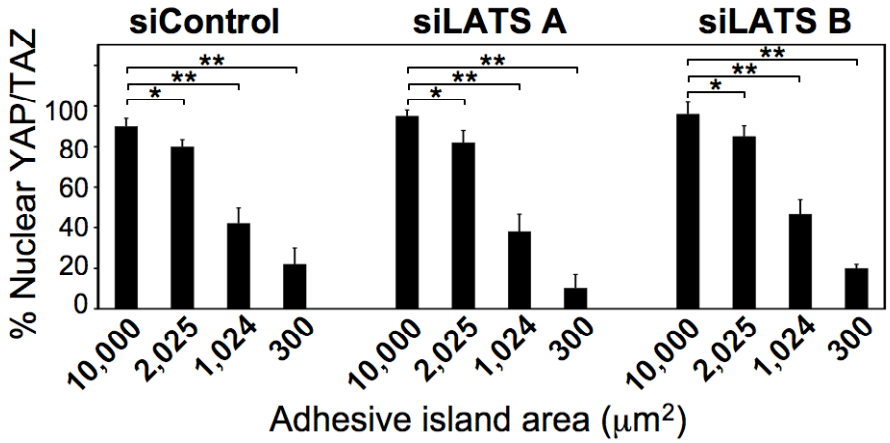

Supplementary Figure 24 | Quantification of nuclear YAP/TAZ in hMSC transfected with control- or LATS-siRNA (with two independent LATS siRNA oligo sets indicated with A and B) and plated on microprinted fibronectin islands. Results with control- and LATS-siRNA #A are the same shown in Fig. 3d of the main text. Data are mean and SD (n=4; **P*<0.05, ***P*<0.01).

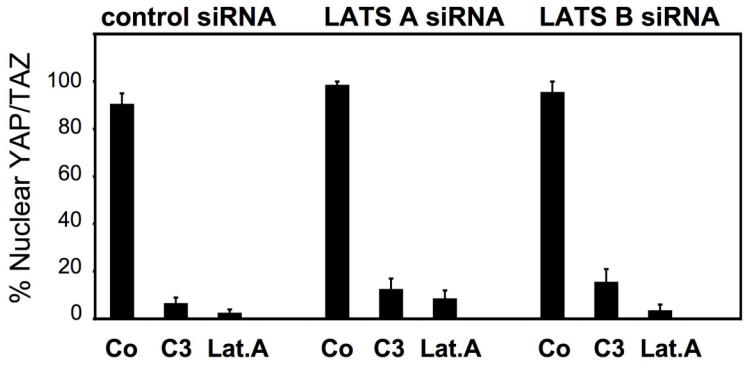

Supplementary Figure 25 | hMSC were transfected with the indicated siRNAs and replated on fibronectin-coated glass. Cells were then treated for 4 hours, where indicated, with the Rho inhibitor C3 or the F-actin inhibitor LatrunculinA (Lat.A), and fixed for IF. Confocal IF images were used to quantify the percentage of cells displaying nuclear YAP/TAZ staining. Data are mean and SD (n=5).

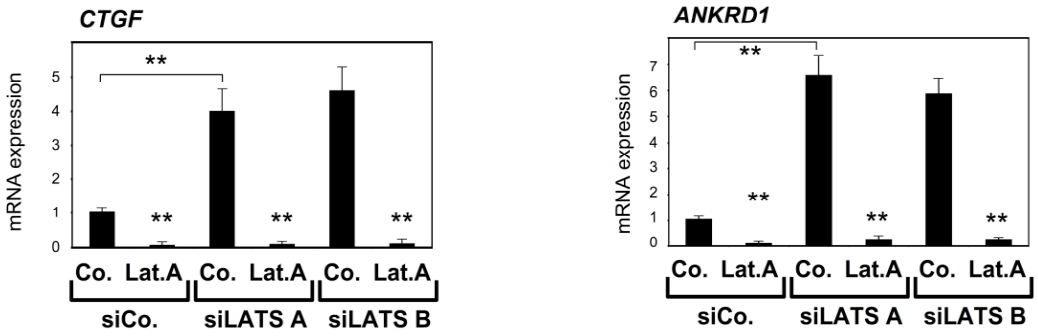

Supplementary Figure 26 | Real-time PCR analysis of the YAP/TAZ transcriptional targets *CTGF* and *ANKRD1* in MCF10A MEC. Cells were transfected with the indicated siRNA and replated at low confluence on fibronectin-coated 40 KPa hydrogels; after 1 day cells were left untreated (Co.) or treated for 24 hours with the F-actin inhibitor LatrunculinA (Lat.A), and harvetsed for qRT-PCR. Data are mean and SD (n=3; $^{**}P<0.01$). The experiments shown here were performed together with the ones shown in Fig. 3f of the main text, such that the untreated samples of this panel (Co.) are the same bars of the controls lanes in Fig. 3f (40KPa).

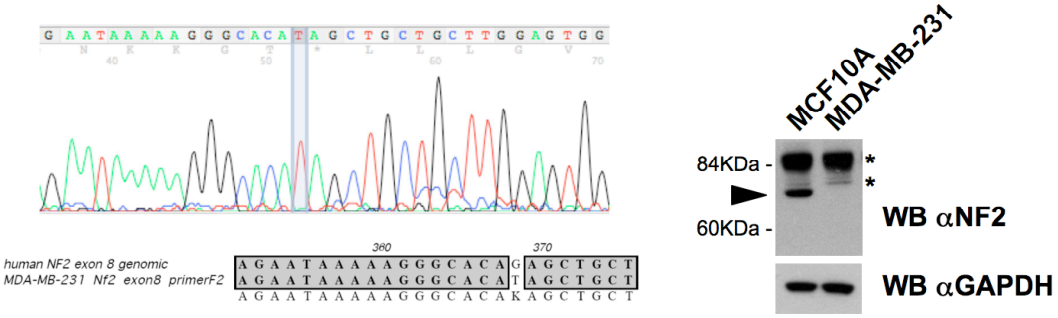

Supplementary Figure 27 | LEFT: Sequencing of the genomic locus of *NF2/merlin* in MDA-MB-231 cells reveals a non-sense mutation within exon8, causing a stop codon (*). Below the chromatogram, the alignment of the nucleotide sequences of MDA-MB-231 cells and the consensus human genome (NCBI) encompassing the mutation is shown. All other exons were normal (not shown). Likely due to nonsense mRNA decay, we could not detect *NF2* mRNA by RT-PCR in MDA-MB-231 cells, as compared to MCF10A (not shown). RIGHT: Western blotting of MCF10A and MDA-MB-231 cell extracts for NF2/merlin (indicated by the black arrowhead). The anti-NF2 antibody recognizes two additional bands (indicated by asterisks) that are aspecific as judged by anti-NF2 siRNA transfection (not shown).

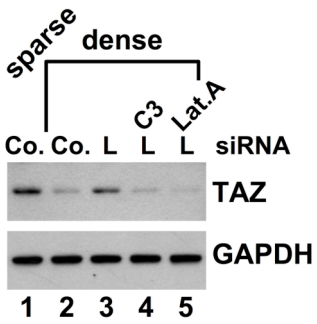

Supplementary Figure 28 | Panel shows western blotting of lysates from MCF10A cells transfected with control siRNAs (Co.) and cultured under sparse and confluent (dense) conditions (lanes 1 and 2). Confluent cells transfected with LATS siRNA #A (L) were either left untreated (lane 3) or treated with C3 or LatrunculinA (Lat.A) for 6 hours before harvesting (lanes 4 and 5).

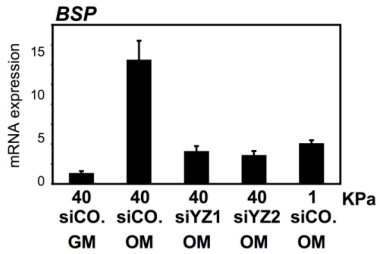

Supplementary Figure 29 | Real time PCR for the osteogenic marker *BSP (bone sialoprotein)* on hMSC. Cells were transfected with the indicated siRNAs, plated on hydrogels of 40 or 1KPa, and either left in growth medium (GM) or induced to differentiate (OM – see methods). Data are mean and SD (n=2).

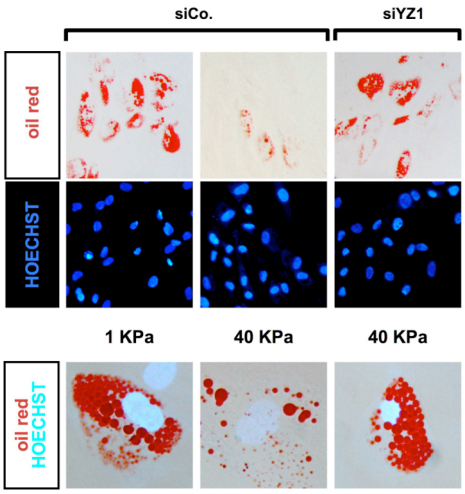

Supplementary Figure 30 | Top row: low magnification pictures of representative oil-red stainings of hMSC whose quantification is showed in Fig. 4c. Hoechst staining shows nuclei of the same cells of the oil-red pictures above. Bottom row: close-up of representative differentiated hMSC. Note how the differences in adipogenic differentiation between samples were not only quantitative (i.e. number of cells displaying oil-red staining) but also qualitative (i.e. amount of vacuoles per cells).

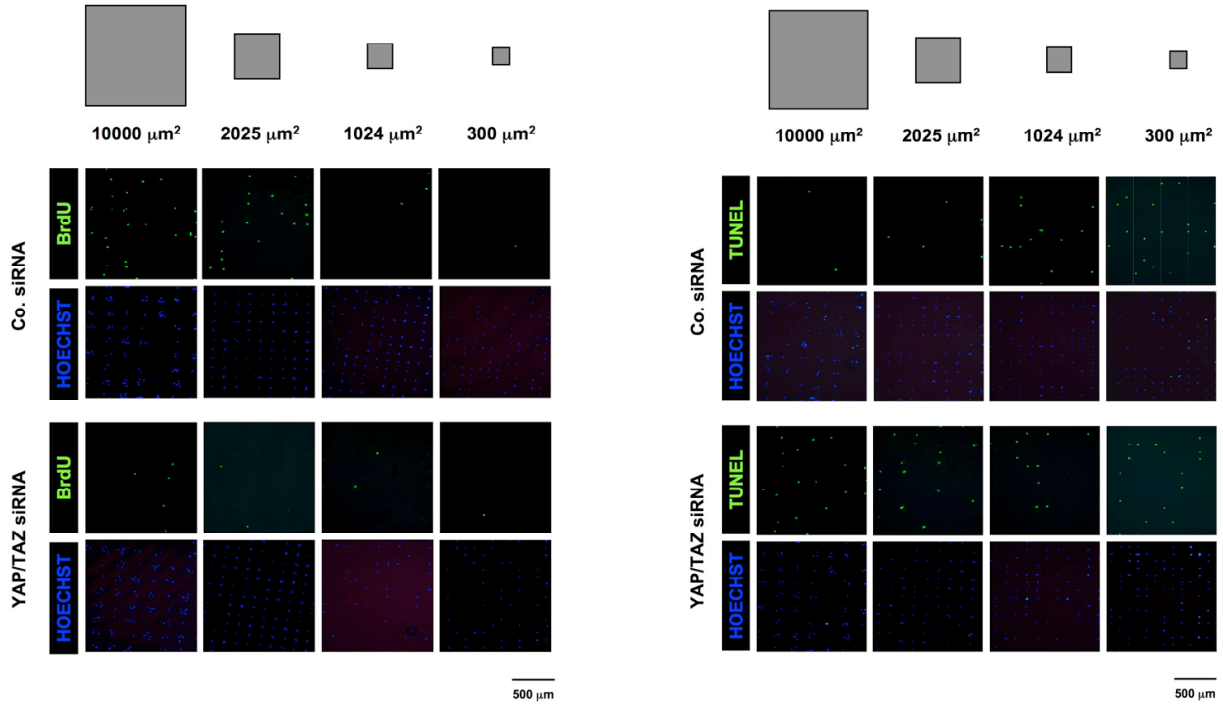

Supplementary Figure 31 | Representative BrdU stainings (LEFT) and TUNEL stainings (RIGHT) of HMVEC whose quantification is showed in Fig. 4d. Hoechst staining (in blue) shows nuclei of the corresponding fields. Gray squares on top show the relative dimensions of the single patterns where cells were seeded on; the black bar at the bottom right serves as scale bar for the pictures.

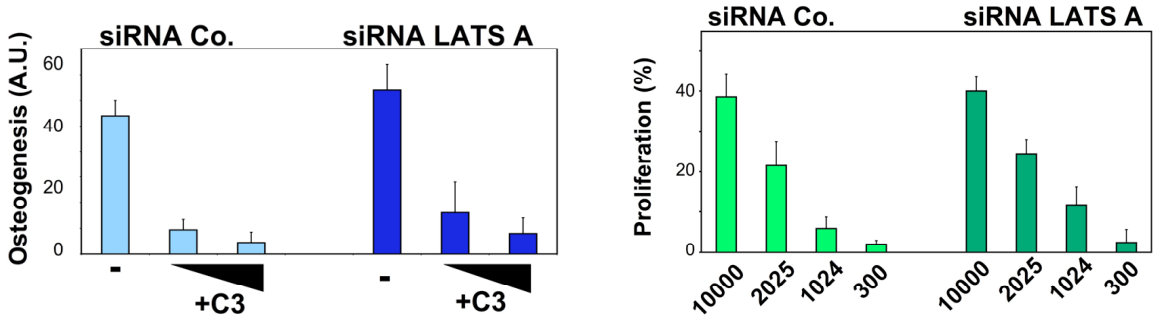

Supplementary Figure 32 | LEFT**:** Quantifications of osteogenic differentiation of control siRNA (siRNA Co.) and LATS siRNA (siRNA LATS A) transfected hMSC. Cells were transfected, replated, and induced to differentiate in the absence (-) or in the presence of increasing doses of the Rho inhibitor C3 (+C3; low dose = 50ng/ml, high dose = 150ng/ml). RIGHT: Quantifications of proliferation of HMVEC transfected with the indicated siRNAs and plated on adhesive islands of different sizes, indicated below each column (μm^2). All data are mean and SD (n=3).

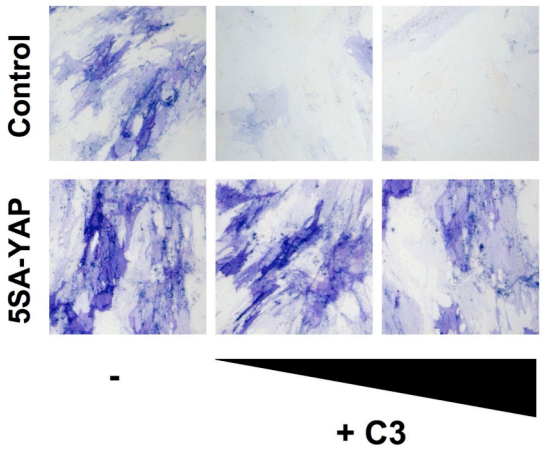

Supplementary Figure 33 | Representative alkaline phosphatase stainings of the experiments quantified in Fig. 4f. C3, Rho inhibitor used at 50 and 150 ng/ml.